ELSEVIER

Advances in Water Resources 23 (2000) 325–337

Advances in Water Resources

Wave-induced beach groundwater flow

L. Li *, D.A. Barry

School of Civil and Environmental Engineering and Contaminated Land Assessment and Remediation Research Centre, The University of Edinburgh, Edinburgh EH9 3JN UK

Received 12 February 1999; received in revised form 1 July 1999; accepted 12 July 1999

Abstract

Wave-induced beach groundwater flow has been linked to sediment transport in the near-shore zone and chemical transfer from the aquifer to the ocean. The flow dynamics, however, are not well-understood. This paper presents a numerical study of the instantaneous (i.e., phase-resolved) wave motion and resulting groundwater responses in the beach zone. Simulations conducted for a representative beach reveal various important features of the flow. In particular, periodic local groundwater circulation occurs below progressive bores while the averaged flow behaviour is characterised by continuous circulation (due to wave set-up) extending from the upper part of the beach to the lower part. These results are analysed and compared with previous analytical solutions derived for simplified situations. The findings will assist future studies to quantify the effects of beach groundwater flow on other coastal processes.

Keywords: Beach groundwater flow; Ocean–aquifer interaction; Near-shore wave dynamics

Notation

AMP	amplitude (L)
a	bore amplitude (L)
BP	breaking point
b	$(3\varepsilon/h_0^2)^{1/2}$
d	still water depth at the seaward boundary (L)
F_s	seepage force due to infiltration/exfiltration (MLT^{-2})
g	magnitude of gravitational acceleration (LT^{-2})
H	incoming wave height at the seaward boundary (L)
HWT	High beach water table
h_0	water depth at the bore front (L)
h_1	local aquifer thickness (L)
h_L	landward hydraulic head of the aquifer (L)
I	infiltration/exfiltration rate (LT^{-1})
K	hydraulic conductivity (LT^{-1})
L	the length of the aquifer base (L)
LWT	low beach water table
l	the distance between BP and RM (L)
MWT	middle beach water table
MSL	mean sea level
P	pore pressure ($ML^{-1}T^{-2}$)
RM	maximum run-up
SWE	shallow water equation
s	the slope of wave set-up
T	wave period (T)
t	time (T)
u	horizontal groundwater flow velocity (LT^{-1})
u_w	horizontal water velocity due to waves (LT^{-1})
w	vertical groundwater flow velocity (LT^{-1})
X_r	x coordinate of the moving shoreline (L)
x	coordinate in the cross-shore direction (L)
x_0	x coordinate of the bore centre (L)
z	coordinate in the vertical direction (L)
β	beach angle (Rad)
ϕ	hydraulic head in the aquifer, $P/\rho g + z$ (L)
ψ	stream function (L)
η	depth of water above the beach face (L)
ε	ratio of a to h_0

1. Introduction

Groundwater flow in a coastal aquifer is influenced by the dynamic boundary conditions at the beach face,

* Corresponding author. Tel.: +44-131-650-5814; fax: +44-131-650-6781.

E-mail address: ling.li@ed.ac.uk (L. Li)

0309-1708/00/$ - see front matter
PII: S0309-1708(99)00032-9

which are underlain by sea level oscillations. At a natural coast, mainly tides and waves drive sea level oscillations. The former have long periods, for example, 24 h for a diurnal tide. In contrast, wave periods typically range from a few to tens of seconds. Since the inland damping of the oscillations is inversely related to the period, tidal influences propagate into a coastal aquifer further than wave-induced influences [6]. In other words, the wave effects are confined within the beach zone.

As waves propagate towards the shore, they inevitably become steeper and steeper due to non-linear effects and beach slope. This often leads to wave breaking and the formation of bores [13]. The large slope of the sea surface in the vicinity of a bore results in significant hydraulic gradients that may cause considerable beach groundwater flows locally. Packwood and Peregrine [11] studied bore-induced groundwater flows on a flat, horizontal porous bed. They found that, at the rear of the bore, infiltration (flow into the porous medium) occurs across the bed while exfiltration (flow out of the porous medium) takes place on the front side. The infiltration/exfiltration rates are determined by the bore amplitude, the water depth at the bore front and the thickness of the underlying aquifer.

Also, as a result of wave breaking, the wave energy is dissipated and the radiation stress is reduced shorewards. The radiation stress is defined as the wave-induced force on the water body [2]. The shoreward decrease of the radiation stress leads to an upwards tilt in the mean sea level as shown in Fig. 1, termed "wave set-up" [2]. Longuet-Higgins [8] demonstrated that the mean on-shore pressure gradient due to wave set-up drives a groundwater circulation within the beach zone. Across the beach face, water infiltrates into the coastal aquifer at the upper part of the beach near the maximum run-up (RM), and exfiltration occurs at the lower part of the beach face near the breaking point (BP). The circulation extends below the beach face, to a depth comparable with the distance between the BP and RM.

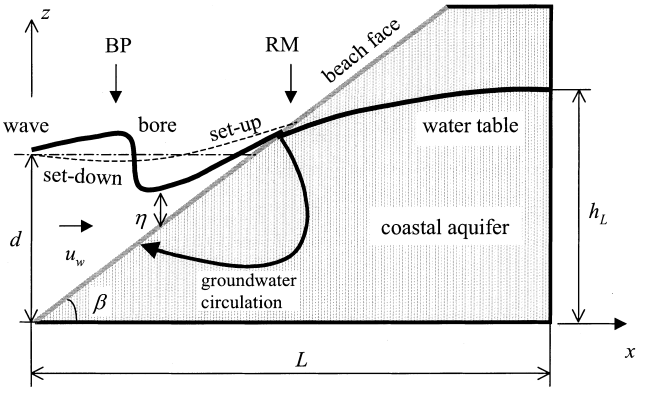

Fig. 1. Schematic diagram of beach processes. Dashed line is the mean sea level and the dot-dashed line shows the still seawater level.

The beach groundwater flow, as induced by wave motion, has been linked to the sediment transport process [1,3,14,15]. Turner and Masselink [15] found that the infiltration/exfiltration in the swash zone (defined as the zone where wave run-up, i.e., upwash, and run-down, i.e., backwash, occur) can increase the sediment transport rate by up to 40% of the peak transport rate during upwash and decrease it by 10% during the backwash. Li et al. [7] demonstrated that the beach groundwater circulation due to wave set-up contributes largely to the submarine groundwater discharge and so affects the chemical transfer from the coastal aquifer to the coastal sea. Despite its importance in these coastal processes, the beach groundwater flow has not been studied to any great extent. Previous studies on dynamics of beach groundwater have been focussed on the behaviour of the water table instead [1]. Longuet-Higgins' analytical solution [8] for the beach groundwater circulation due to wave set-up did not include the free-surface boundary conditions at the water table or the landward hydraulic condition. Thus, its applicability to natural beaches may be restricted. Little is known about the responses of the beach groundwater to a bore and how the responses vary in the surf and swash zones.

As a bore propagates on the beach, its amplitude and front water depth will vary, as will the thickness of the underlying local aquifer. The bore-induced beach groundwater flow is, therefore, expected to behave differently from that predicted by Packwood and Peregrine's analytical solution [11]. Recently, Turner and Masselink [15] reported a field study of the instantaneous infiltration/exfiltration in the swash zone. While the study provided, for the first time, data of the instantaneous flow rates across the beach face, the measurements were limited to a single location. The overall dynamics of the beach groundwater flow are yet to be investigated.

The objective of the present study is to examine, through numerical modelling, the basic features of instantaneous and phase-averaged beach groundwater flows induced by waves. The instantaneous flow will reveal the groundwater responses to bores and wave run-up. It will be simulated using phase-resolved waves. The numerical results will be compared with Packwood and Peregrine's analytical solution [11] with the aim of testing the applicability of the latter in the case of a sloping beach. The phase-averaged flow, obtained by averaging the instantaneous flow over a wave cycle, will depict the groundwater circulation due to wave set-up (also a phase-averaged phenomenon). The simulations are conducted using an existing numerical model [6]. The model simulates the interacting wave motion and groundwater flow (Fig. 1). The non-linear shallow water equation (SWE) was used to describe the wave motion on the beach. Only the saturated groundwater flow in the aquifer, as governed by the Laplace equation, was

considered in the model. However, capillary effects on saturated flow are incorporated through the free-surface boundary conditions at the water table (cf. [12]). The dynamic boundary conditions at the beach face for the groundwater flow were determined by the elevation of the sea surface as computed by the SWE. This model has been used to simulate the water table's responses to wave run-up and was found to reproduce the behaviour of observed high frequency water table fluctuations [6]. Further details of the model are provided in Appendix A.

In the following sections, simulation results of the instantaneous and phase-averaged beach groundwater flow will be presented and discussed.

2. Instantaneous beach groundwater flow

The values of the model parameters used in the simulation are listed in Table 1. The incoming waves specified at the seaward boundary were of a sinusoidal form with $H = 0.5$ m and $T = 6$ s. The beach slope remained at 0.1 during the simulation, i.e., no changes in beach topography were considered. The landward hydraulic head of the groundwater was set to be 2.3 m, which would not lead to large net groundwater flows (either landward or seaward). These parameter values are realistic; for example, the values of the wave period and beach slope are typical for macro-tidal beaches in Australia [10]. The simulation started with a still seawater level at a height of $z = 2$ m and was run for 12 wave periods to ensure that the effects of the initial condition were forgotten. The results from the last period are used for the analysis presented below.

2.1. Bore-induced beach groundwater flow

The simulated wave profiles, in a sequence for $t = 2.64$, 3.74, 5.94 and 7.05 s (from the beginning of the last wave), are shown in Fig. 2a. At $t = 2.64$ s, the wave "broke" and formed a bore at approximately $x = 10$ m. The bore then propagated towards to the shore and ran up the beach. In the vicinity of the bore, a large gradient in the hydraulic head exists, leading to local beach groundwater flows. Infiltration occurred across the beach face on the backside of the bore while exfiltration took place below the bore front (Fig. 2b). The rates of

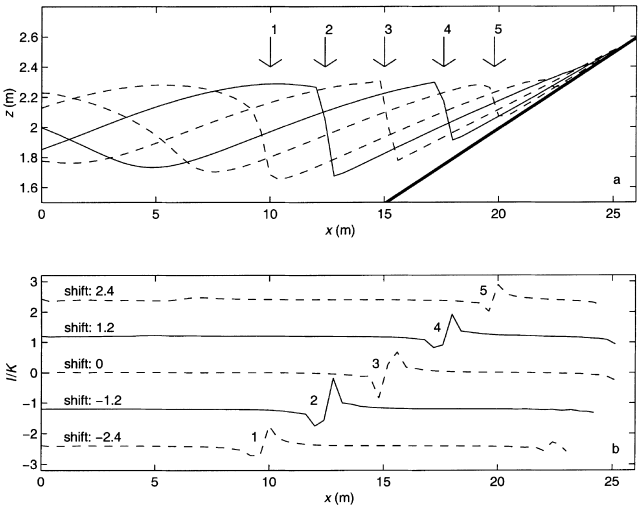

Fig. 2. Simulated wave profiles (a) and infiltration/exfiltration (b). The arrows indicate the bore fronts. To separate the curves of the infiltration/exfiltration rates at different times, we have shifted each of them by the increment shown in b.

infiltration and exfiltration varied in response to changes in the bore amplitude, the front water depth and the aquifer thickness. However, the infiltration–exfiltration pattern remained unchanged and propagated across the shore with the bore. Note that negative I means infiltration and positive I denotes exfiltration according to the coordinates as defined. To clearly display the results, we shifted the infiltration/exfiltration curves at different times by the increments as shown in Fig. 2b. The flow pattern is very similar to that of bore-induced groundwater flow across a flat horizontal porous bed (Fig. 3). Packwood and Peregrine [11] derived analytical solutions for the latter phenomenon by solving the Laplace equation for groundwater flow subject to the boundary condition at the bed as described by (1). This boundary condition reflects the hydraulic head variations due to a bore,

$$\eta = h_0 + \frac{a}{2}\{1 - \tanh[b(x - x_0)]\}, \tag{1}$$

where h_0 is the water depth at the bore front, a the bore amplitude, x_0 the coordinate of the bore centre and $b = (3\varepsilon/4h_0^2)^{1/2}$ with $\varepsilon = a/h_0$. Analytical solutions were obtained for shallow and deep aquifers, respectively. The aquifer's shallowness is defined as $h_1 b$ (the ratio of the aquifer thickness to the horizontal characteristic

Table 1
Parameter values used in the simulations

SIM number	Model parameters						
	H (m)	T (s)	d (m)	L (m)	h_L (m)	K (m/s)	tan (β)
1 (MWT)	0.5	6	2	60	2.3	0.001	0.1
2 (HWT)	0.5	6	2	60	2.6	0.001	0.1
3 (LWT)	0.5	6	2	60	1.5	0.001	0.1

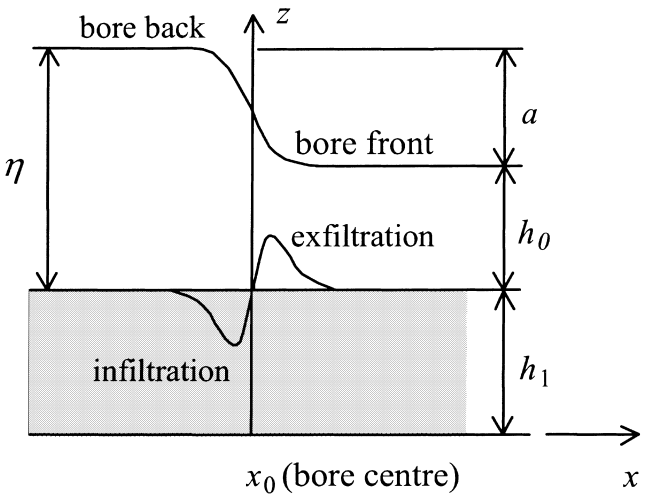

Fig. 3. Schematic diagram of the bore and the groundwater flow across a flat horizontal porous bed.

length scale, $1/b$). For a shallow aquifer (i.e., $h_1 b$ is small), the bore-induced vertical groundwater flow is given by,

$$\frac{w}{K} = \frac{3\varepsilon^2}{4}\frac{z}{h_0}\tan[b(x-x_0)]\,\mathrm{sech}^2[b(x-x_0)]. \tag{2}$$

This solution indicates that the vertical pressure profile is parabolic. For a deep aquifer (i.e., $h_1 b$ is large), the flow is unaffected by the depth, and

$$\frac{w}{K} = \frac{3\varepsilon^2(x-x_0)}{2h_0}\sum_{n=0}^{\infty}\frac{\pi(n+1/2)}{[b^2(x-x_0)^2+\pi^2(n+1/2)^2]^2}. \tag{3}$$

Two numerical simulations were conducted to examine bore-induced vertical flows across a flat horizontal bed. The results are shown in Fig. 4 and compared with the above analytical solutions. In both simulations, $x_0 = 0$ m, $a = 0.2$ m, $h_0 = 1$ m. A small aquifer thickness, $h_1 = 0.5$ m, was used in the shallow aquifer simulation, giving $h_1 b = 0.19$. For the deep aquifer simulation, $h_1 = 50$ m and $h_1 b = 19$. The agreement between the numerical predictions and analytical solutions is very good for both cases.

Although the beach face is not horizontal, the slope is small and hence the above analytical solutions may be used to predict the local infiltration/exfiltration caused by bores on the beach. We first examined the simulated beach groundwater flow at $t = 2.86$ s (when the bore is located near the BP) in the light of the above analytical solution. From the wave profile, we estimated the bore amplitude a to be 0.63 m. By fitting Eq. (1) to the simulated bore (Fig. 5a), we determined the bore centre to be at $x_0 = 10.2$ m. Eqs. (2) and (3) were then used to predict the groundwater flow at the beach face. The results, shown in Fig. 5b, indicate that the shallow aquifer solution provides a good prediction of the numerical data. In particular, the predicted maximum infiltration and exfiltration rates matched the numerical results well, as did the locations of those maxima. In comparison, the deep aquifer solution underestimated the magnitude of the infiltration/exfiltration rates. At the lower part of the beach, the aquifer is relatively shallow ($h_1 b = 1.4$) and hence good performance of the shallow aquifer solution is expected. The main difference between the numerical results and the shallow aquifer solution occurred in the back and front of the bore. The infiltration and exfiltration rates predicted by the analytical solution decreased rapidly to zero with the distance from the bore centre while the numerical results showed more gradual changes. Such a difference in the flows is likely to have been transferred from the difference between the simulated and fitted bores, which also occurred in the same areas. In calculating the shallow

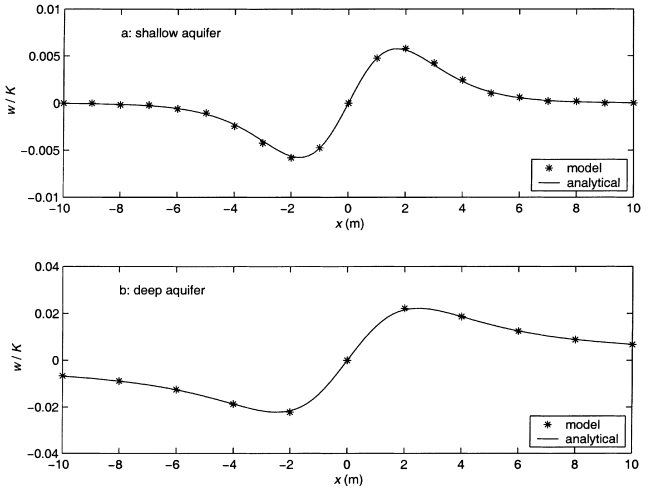

Fig. 4. Comparison of the simulated bore-induced flow across a flat bed with analytical solutions of Packwood and Peregrine [11].

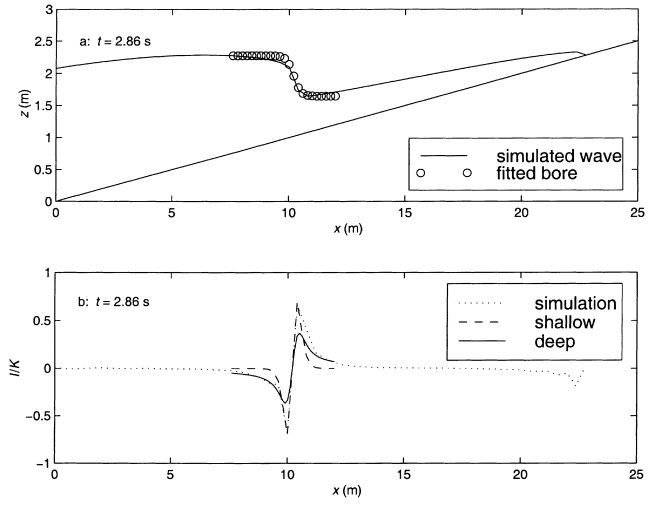

Fig. 5. Comparison of the simulated bore (a) and infiltration/exfiltration (b) with analytical solutions by Packwood and Peregrine [11] for $t = 2.86$ s.

aquifer solutions, we used the local water depth and aquifer thickness at $x = 10.8$ m (i.e., the bore front). Note that at the sloping beach, the bore does not overlay on a uniform water depth. It is also interesting to note that the infiltration and exfiltration are an odd function (i.e., symmetrical) with respect to the bore centre.

From the infiltration–exfiltration flow pattern, one can infer the existence of a local groundwater circulation beneath the beach face in the vicinity of the bore. In Fig. 6, we plotted the hydraulic heads and head gradients inside the beach aquifer. Clearly, the bore caused large horizontal and vertical gradients of hydraulic heads in the aquifer below it. The hydraulic gradients drove a local groundwater circulation, as shown in Fig. 6. To further examine the distribution of the hydraulic heads, we analysed the vertical profiles of the heads at the back ($x = 8$ m) and front ($x = 10.4$ m) of the bore (Fig. 7). The heads at the bore back are higher than those at the front over the entire depth. The former decreased with the depth from the beach face, causing a downward flow while the latter increased with the depth, giving an upward flow. The downward and upward flows are consistent with the infiltration and exfiltration occurring at the two locations, respectively. The vertical head profiles

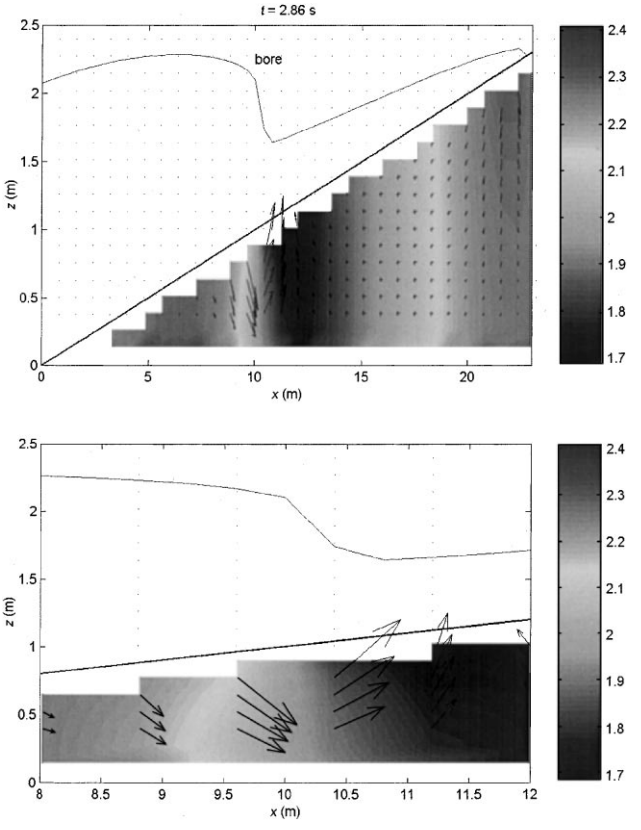

Fig. 6. Local groundwater circulation in the vicinity of the bore. Arrows indicate the head gradients and flow velocities. Colours represent the heads. Lower panel is extracted from the upper panel and focuses on the bore area.

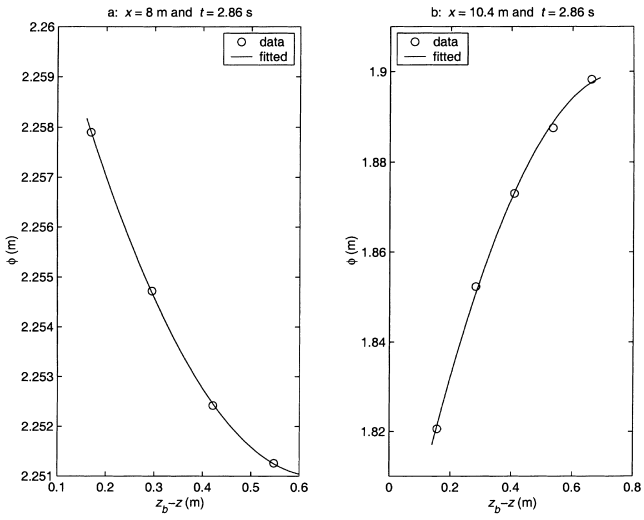

Fig. 7. Vertical head profiles below the bore in the aquifer at $t = 2.86$ s. Results are shown for two locations. Data were fitted with parabolic functions.

at both locations are approximately parabolic as shown in Fig. 7. The fitted curves are $\phi = 0.032(z_b - z)^2 0.040(z_b - z) + 2.264$ for $x = 8$ m and $\phi = -0.216(z_b - z)^2 + 0.328(z_b - z) + 1.772$ for $x = 10.4$ m (where z_b is the elevation of the beach face).

Differentials of ϕ with respect to z give the non-dimensional vertical flow velocity. According to the fitted functions, the magnitude of the vertical flow decreased linearly with the depth from the beach face. This behaviour is in agreement with the analytical solution for a shallow aquifer, Eq. (2). However, the depth-reduction rate of the flow speeds at $x = 8$ m, 0.064 m^{-1}, did not agree with the analytical prediction, 0.005 m^{-1}. Such a difference is again due to the difference between the fitted and simulated bores occurring at the same location. At $x = 10.4$ which is near the bore centre, the numerical prediction of the reduction rate, 0.43 m^{-1}, is close to the analytical estimate, 0.48 m^{-1}.

To examine the applicability of the analytical solution in areas closer to the shore, the above analysis was repeated for $t = 5.06$ s when the bore reached $x = 15.1$ m. The results showed that both the shallow and deep aquifer solutions largely over-predict the infiltration and exfiltration rates (Fig. 8). In this case, the prediction of the deep aquifer solution is closer to the numerical data because the aquifer thickness is large relative to the water depth. Packwood and Peregrine's analytical solutions [11] were derived for a small amplitude bore, i.e., assuming that ε is small. As the bore moves toward the shore, this ratio increases rapidly and hence the analytical solutions fail. Another factor is that water table is likely to affect the flow near the upper part of the beach. Water table effects are not included in the analytical solutions, which were based on a horizontal bed. Although the infiltration/exfiltration rates cannot be

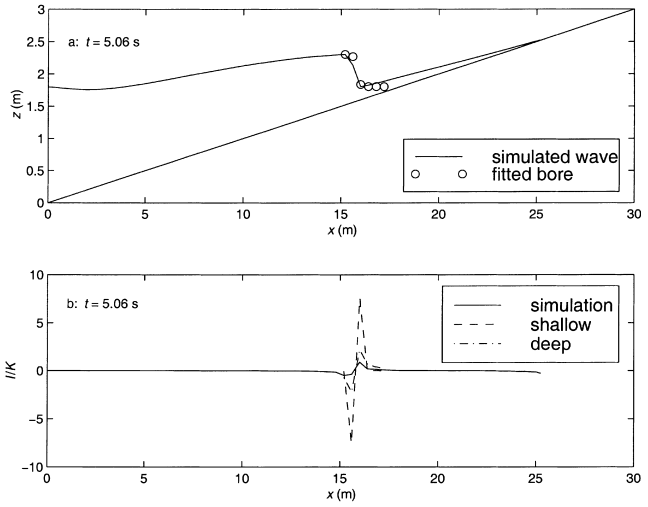

Fig. 8. Comparison of the simulated bore (a) and infiltration/exfiltration (b) with analytical solutions by Packwood and Peregrine [11] for $t = 5.06$ s.

predicted by the analytical solution, the local flow patterns, including the symmetrical infiltration/exfiltration across the beach face and the groundwater circulation in the aquifer, are similar to those in the lower part of the beach. The vertical head profiles were also found to be approximately parabolic (Fig. 9), consistent with the Eq. (2).

In summary, the analytical solution developed for a flat horizontal bed and shallow aquifer can be used to predict bore-induced beach groundwater flow at the lower part of the beach provided that local parameters (i.e., ε, h_0 and h_1) are used. This approach is not valid for upper part of the beach where ε is large and the water table effects are important.

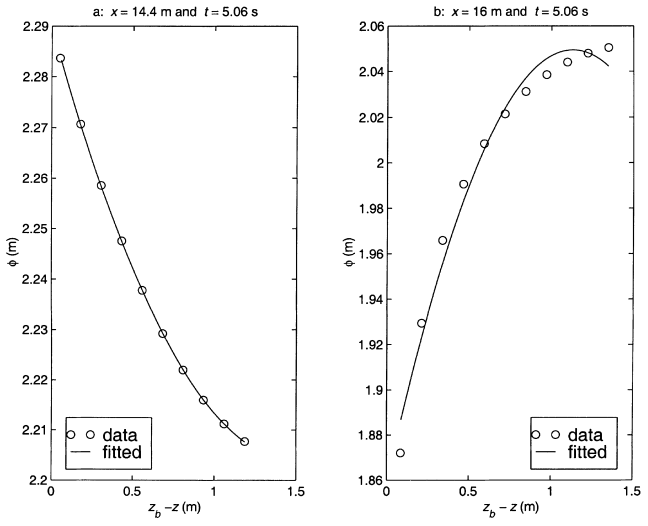

Fig. 9. Vertical head profiles below the bore in the aquifer at $t = 5.06$ s. Results are shown for two locations. Data were fitted with parabolic functions.

2.2. Cross-shore variations of the bore-induced beach groundwater flow

As the bore propagates towards the shore, its amplitude decreases due to energy dissipation. However, the ratio of the bore amplitude to the water depth increases and so does the thickness of the aquifer. The beach groundwater flow varies in response to these changes. To examine such variations, we focussed on the maximum infiltration/exfiltration rates, which represent the magnitudes of the local beach groundwater flow.

Fig. 10a shows the bore amplitude as it varies with location. The first data point may only represent a very steep wave front prior to breaking. Such a steep wave front induces beach groundwater flow similar to that due to a bore and thus is also included in the analysis. The water depth and the aquifer thickness are shown in Fig. 10b and c, respectively. The non-dimensional maximum infiltration/exfiltration rates were plotted in Fig. 10d.

The magnitude of the beach groundwater flow reaches a maximum at $x = 13$ m, which does not coincide with the BP where the bore has its highest amplitude. We first used Eq. (2) to relate the magnitude of the beach groundwater flow to the bore condition and aquifer thickness, i.e.,

$$\left(\frac{w}{K}\right)_{\max} = 0.385\frac{3\varepsilon^2}{4}\frac{h_1}{h_0}, \quad z = h_1 (\text{i.e., flow across the bed as shown in Fig. 3}) \tag{4}$$

where 0.385 is the maximum of $\tanh(bx)\,\mathrm{sech}^2(bx)$. The results show that Eq. (4) can be used to quantify the magnitude of the infiltration/exfiltration at the lower part of the beach, i.e., seaward of $x = 13$ m (Fig. 11a).

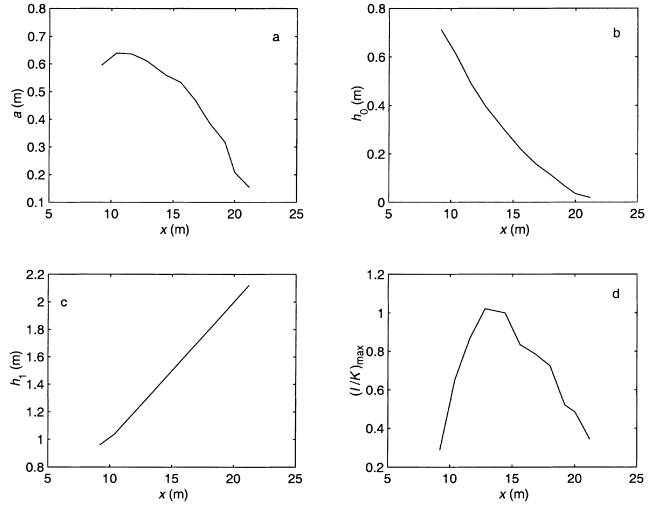

Fig. 10. (a) Variations of bore amplitude with bore location (centre). (b) Water depth of bore front. (c) Aquifer's thickness at the bore front. (d) Variations of the magnitude of infiltration/exfiltration (the maximum infiltration/exfiltration rate) with bore location.

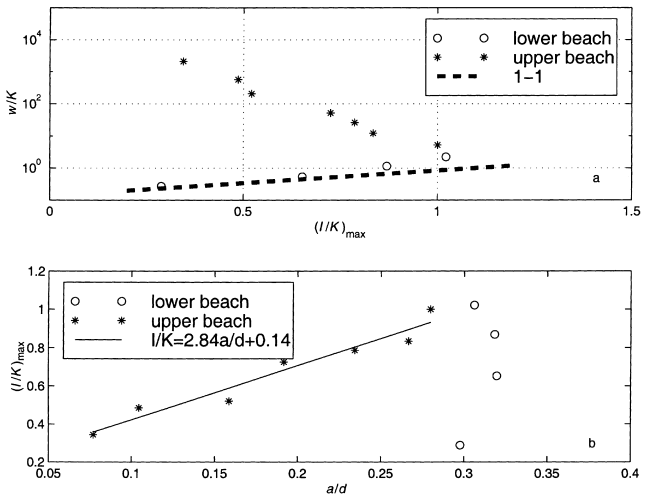

Fig. 11. (a) Comparison of the numerical prediction of the maximum infiltration/exfiltration rate with that of the analytical solution for a shallow aquifer. (b) Relation between the maximum infiltration/exfiltration rate and the bore amplitude. Circles are data for lower beach and stars for upper beach. The dashed line in (a) shows that the maximum infiltration/exfiltration at lower part of the beach can be predicted by the analytical solution. The solid line in (b) indicates that the maximum infiltration/exfiltration rate at upper part of the beach is linearly related to *a/d*.

At the upper part of the beach, the magnitude of the infiltration/exfiltration is not described by Eq. (4); instead, it is linearly related to the bore amplitude (Fig. 11b). It is interesting to note that the location separating these two different behaviours of I coincided with the location where the magnitude of the beach groundwater flow reaches the maximum (i.e., $x = 13$ m).

It is well-known that the infiltration/exfiltration induces a seepage force on the beach sediment. In particular, an upward force acts on the sediment as a result of exfiltration. The magnitude of this force is related to the flow rate [9,15],

$$F_s = \frac{1}{2}\frac{I}{K}\rho g, \tag{5}$$

where F_s is the magnitude of the seepage force, ρ the water density and g is the magnitude of the gravitational acceleration. According to the simulation, I/K can be as high as unity (e.g., Fig. 10d) and hence the seepage force due to exfiltration may amount to one third of the sediment's immersed weight. This obviously has important implications for sediment suspension in the surf zone.

2.3. Cyclic infiltration/exfiltration and head fluctuations caused by bores' passage

In Fig. 12a, we show the infiltration and exfiltration at $x = 10.4$ and 16 m over two wave periods. The time-variations of the local beach groundwater flow are characterised by cycles of exfiltration and then infiltration following the passage of bores. First, exfiltration occurred as the bore approached and the front reached the location. Subsequently, infiltration started as the bore centre moved shoreward. Without the bore nearby, the beach groundwater flow is relatively small.

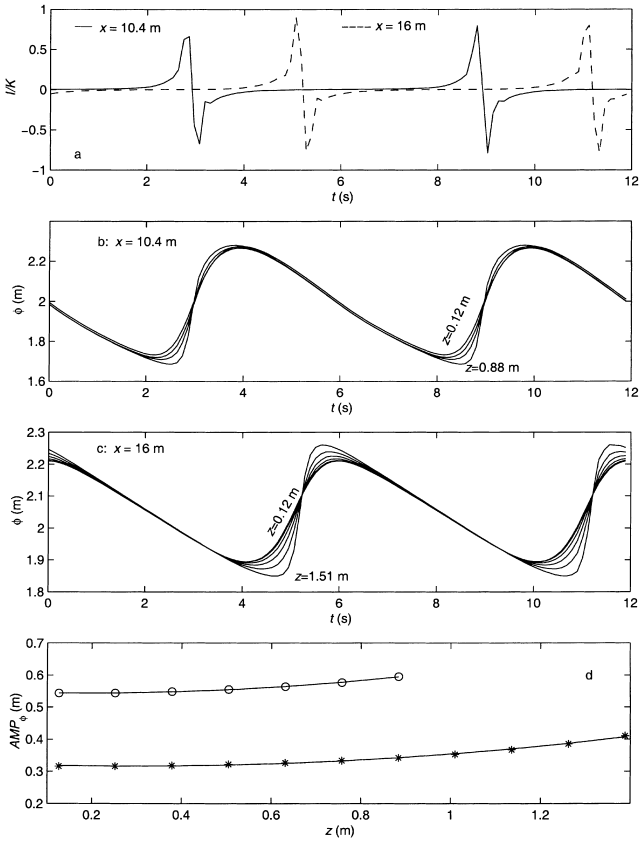

Fig. 12. (a) Time-variations of infiltration/exfiltration at fixed locations. (b) Head fluctuations at different depths for $x = 10.4$ m. (c) head fluctuations at different depths for $x = 16$ m. (d) depth variations of the amplitude of head fluctuations at $x = 10.4$ m (circles) and $x = 16$ m (stars).

Accordingly, the hydraulic heads in the aquifer at these locations fluctuated, as shown in Fig. 12b and c. Prior to the passage of the bore, the hydraulic heads declined with time and there was little head variation with depth. As the bore approached, the depth variations of the heads were enlarged. The hydraulic heads in the deep areas (e.g., $z = 0.12$ m) became considerably higher than those in the shallow areas (e.g., $z = 0.88$ m), resulting in an upward flow. As the bore passed, the hydraulic heads in both deep and shallow areas rose quickly. The head increase in the shallow areas was more rapid than in the deep areas. Consequently, the heads near the beach face became higher than those in the deep areas, resulting in downward flow. Afterwards, the heads declined again and their variations over the depth were much reduced. These features of the head fluctuations are consistent with the behaviour of the infiltration/exfiltration across the beach face.

The results indicate that the amplitude of the head fluctuations decreases with depth ($z_b - z$). We calculated the amplitude from the head fluctuations at different depths and found that the decrease follows a parabolic trend (Fig. 12d). This is in agreement with previous results of the vertical head profiles. The results also exhibit time lags between the fluctuations at different depths. During the first phase of the bore passage (i.e., prior to the passing of the bore centre), the head fluctuation in the shallow area lagged behind that in the deep areas. This is due to the fact that the head changes are caused by an upward flow. The opposite occurred during the second phase, in which case the head changes result from downward flow.

2.4. Beach groundwater flow in the swash zone

After the bore reaches the shore, it will run up and down the beach face. The area where the run-up (upwash) and run-down (backwash) is the swash zone. The simulated shoreline is plotted in Fig. 13, and shows clearly the upwash and backwash motion in the swash zone that spanned between $x = 22.9$ and $x = 25.1$ m. The analysis below will focus on the middle of the swash zone, i.e., $x = 23.92$ m.

The swash depth at this location is shown in Fig. 14a. As the swash lens (a thin layer of water undergoing upwash and backwash) retreats seaward, the swash depth becomes zero. The upwash swash depth increases rapidly, reaches a maximum, then decreases gradually to zero. The hydraulic heads in the aquifer follow a similar trend (Fig. 14b). While the swash lens covers the beach face, the vertical head gradients are downward. The magnitude of the head gradient at a fixed depth varies little with time, despite the changes of the swash depth and heads. As the swash lens retreats and the swash depth reduces to zero, the heads likewise decline, the latter being more rapid near the beach face than in the deep areas. This results in a switch of the direction of the head gradient from downward to upward. The variations of the infiltration/exfiltration across the beach, as shown in Fig. 14c, are consistent with the behaviour of the hydraulic heads and the head gradients. In particular, at a given location, a steady infiltration rate

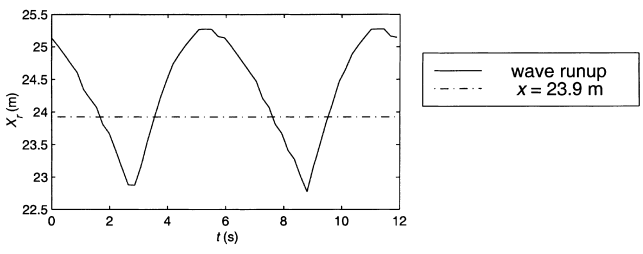

Fig. 13. Simulated wave run-up. Dot-dashed line indicates the middle of the swash zone.

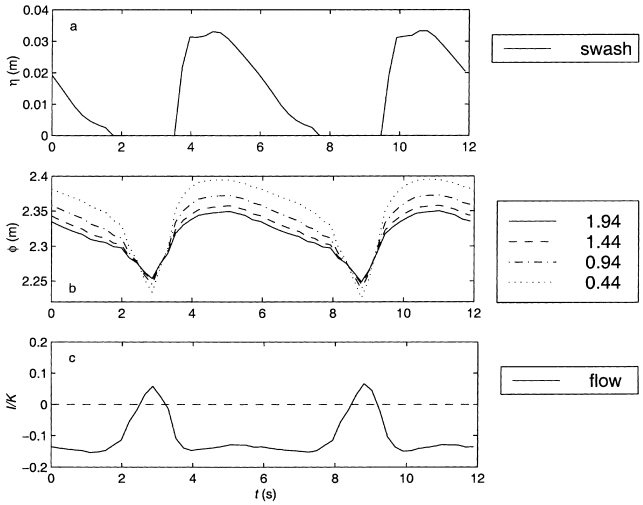

Fig. 14. (a) Simulated swash depth at $x = 23.9$ m over two wave periods. (b) Head variations at different depths (i.e., $z_b z$; the values are listed in the legend box). (c) Time-varying rates of local infiltration/exfiltration.

persists while the swash lens is present. Exfiltration occurs during the dry period (i.e., zero swash depth). It is clear from the results that, in the swash zone, infiltration is dominant and the averaged flow is downward. The behaviour of the phase-averaged flow will be discussed further in the next section.

The flow variations in the aquifer with the time and depth are shown in Fig. 15. The behaviour of the vertical flow (Fig. 15a), especially near the beach face, mirrors that of the infiltration/exfiltration shown in Fig. 14c. The magnitudes of both the downward and upward flows decreased with depth. To examine such a decrease of the vertical flow rates, we selected two data sets for the wet (non-zero swash depth) and dry (zero swash depth) periods, respectively. In both cases, the reduction of the downward and upward flow rates with the depth seemed to be linear (Fig. 15b), a feature similar to that of bore-induced flow as predicted by Eq. (2).

The horizontal flow is also shown in Fig. 15c and d. The rates of the horizontal flow appeared to be more variable with time compared with the vertical flow rates, especially during the wet period. In other words, swash depth variations affected the horizontal flow. The downward vertical flow during the wet period was found to be associated with a seaward horizontal flow, and the upward vertical flow with a landward horizontal flow. The former association was essentially due to the tilt of the sea level, which induced not only a downward but also a seaward hydraulic gradient. The latter association indicated that the upward flow was caused by the approach of the upwash lens (coming from the seaward side), which generated a landward hydraulic gradient, similar to that due to a bore. The time-averaged flows at all depths were seaward. This is due to the effects of

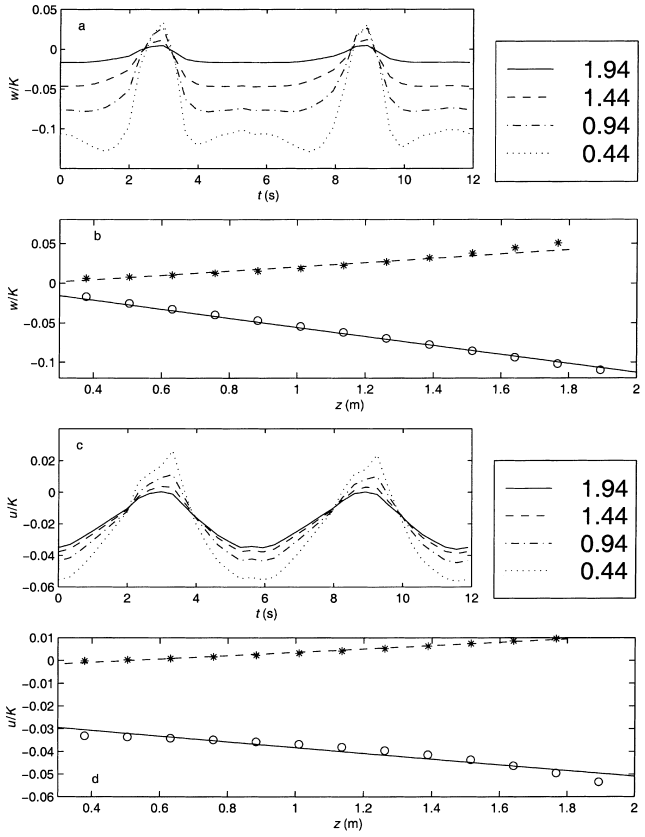

Fig. 15. (a) Simulated vertical flows at different depths. Values shown in the legend box are the depths from the local beach face. (b) Variations of the vertical flow rates with depth. Circles are for $t = 0.22$ s and stars for $t = 2.86$ s. (c) Simulated horizontal flows at different depths. (d) Variations of the horizontal flow rates with depth. Circles are for $t = 0.22$ s and stars for $t = 2.86$ s.

wave set-up and will be discussed in the next section. The rates of the horizontal flow also decreased with the depth in a manner similar to that of the vertical flow rates (Fig. 15d).

A comparison of the vertical and horizontal beach groundwater flows in the swash zone indicates that these two flows are of similar magnitude though the former is higher. We can compare this result with the assumption [15] that the horizontal head gradients within the beach face are several orders of magnitude smaller than the vertical head gradients. It should be pointed out that Turner and Masselink [15] reported only measurements along a single vertical transect in the swash zone, i.e., there were no cross-shore measurements. In an attempt to quantify the vertical flow and the head variations at the measurement location, they used a one-dimensional model, i.e., $w = -K\,\mathrm{d}\phi/\mathrm{d}z$. The authors assumed the local aquifer thickness to be 2 m and took the boundary conditions at the aquifer base to be no vertical flow. This simple model, however, does not account for the horizontal flow. Since $w = 0$ at the base, $\mathrm{d}w/\mathrm{d}z$ over the depth is non-zero and may be estimated as I/h_1 (h_1 is the local aquifer thickness, i.e., 2 m for the data of Turner and Masselink [15]). Mass conservation requires that $\mathrm{d}u/\mathrm{d}x \sim I/h_1$ ($\sim$ means same order of magnitude). Clearly, the characteristic length scale for the horizontal flow (e.g., the distance between two subsequent bores) is of the same order of magnitude as h_1 and hence $u \sim I$. In other words, the magnitude of the horizontal flow is the same as that of the vertical flow, in agreement with the present numerical results. It is interesting to note that the magnitude of the instantaneous beach groundwater flow in the swash zone is much less than that of the bore-induced groundwater flow in the surf-zone.

3. Phase-averaged beach groundwater flow

The mean sea level was calculated by averaging the simulated instantaneous wave profile. A wave set-down and set-up appeared seaward and landward of the BP, respectively (Fig. 16a). Wave set-down is referred to the downward tilt of the mean sea level due to shoaling effects [1]. The phase-averaged infiltration/exfiltration rates were also obtained by averaging the simulated instantaneous flows over a wave period (Fig. 16b). The results show that, driven by the hydraulic gradient due to wave set-up, infiltration occurred at the upper part of the beach near the RM and exfiltration took place at the lower part of the beach near the BP. Below the beach face, groundwater circulated as shown by the path-lines in Fig. 16c. The averaged flows in the aquifer (indicated by arrows) were calculated by averaging the instantaneous flows from the simulation. Again, we see that the horizontal and vertical flow rates are of similar magnitude.

Longuet-Higgins [8] provided an analytical solution for the groundwater circulation induced by wave set-up (Fig. 17),

$$\phi = sl\exp(-\xi)\cos(\gamma), \tag{6a}$$

$$\psi = sl\exp(-\xi)\sin(\gamma), \tag{6b}$$

$$x = l\cosh(\xi)\cos(\gamma), \tag{6c}$$

$$z = l\cosh(\xi)\sin(\gamma), \tag{6d}$$

where ψ is the stream function; x' and z' are the local coordinates, as defined in Fig. 17; ξ and γ are the elliptical coordinates transformed from x' and z' according to Eqs. (6c) and (6d); l is the distance between the BP and the RM and s the slope of the wave set-up. The analytical solution assumed the following boundary conditions,

$$\frac{\partial\phi}{\partial x'} = \begin{cases} s(\text{constant}) & \text{between BP and RM,} \\ 0 & \text{elsewhere on the beach face.} \end{cases} \tag{7}$$

The problem was solved for a semi-infinite domain. In other words, the effects of the water table, aquifer's

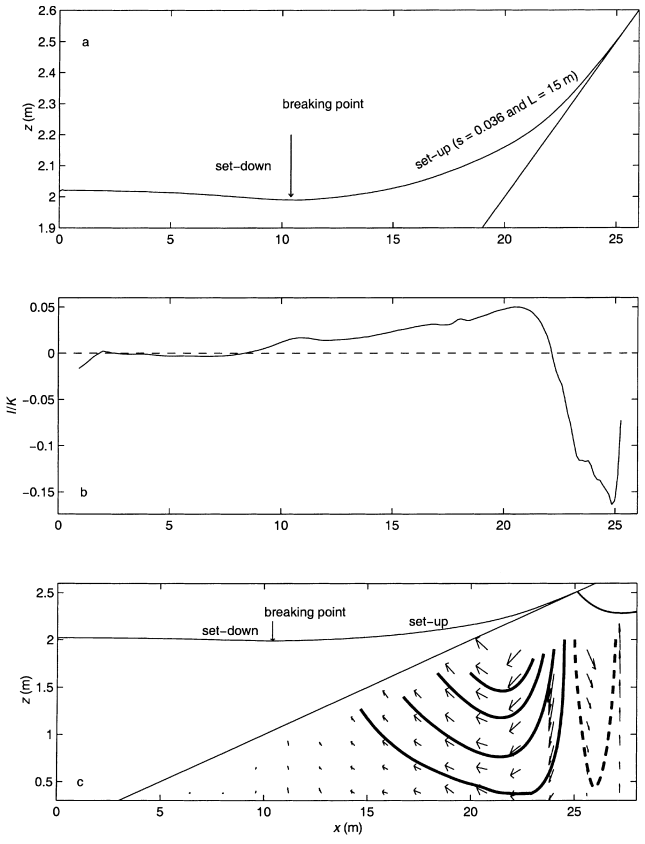

Fig. 16. (a) Mean sea level. (b) Averaged infiltration/exfiltration rates. (c) Averaged beach groundwater flow. Curves in the aquifer are path-lines shown the groundwater circulations.

bottom and landward boundaries were not included in the analytical solution.

The pattern of the groundwater circulation given by the analytical solution (Fig. 17) has some features that can be found in the numerical simulation (Fig. 16c). The simulated circulation started with infiltration in the swash zone and ended with exfiltration at the lower part of the beach. Inner circulation cells, near the beach face, were small in comparison with outer cells that extended below the beach face to areas near the aquifer's bottom boundary and spanned the RM and BP. The main difference between the numerical and analytical results is that, in the former, the circulation cells were not symmetrical with respect to the local z' axis across the middle between RM and BP. The inflow was concentrated within a small area near RM while the outflow spread over a larger area (Fig. 16b and c). These differences are likely due to the effects of the water table, the aquifer's base and landward boundary, which were neglected in the analytical solution. Landward of the beach groundwater circulation, there is an internal circulation below the beach water table (dashed path-line in Fig. 16c). The horizontal extent of this circulation was between $x = 25$ and $x = 28$ m, relatively small compared with that of the beach groundwater circulation. The

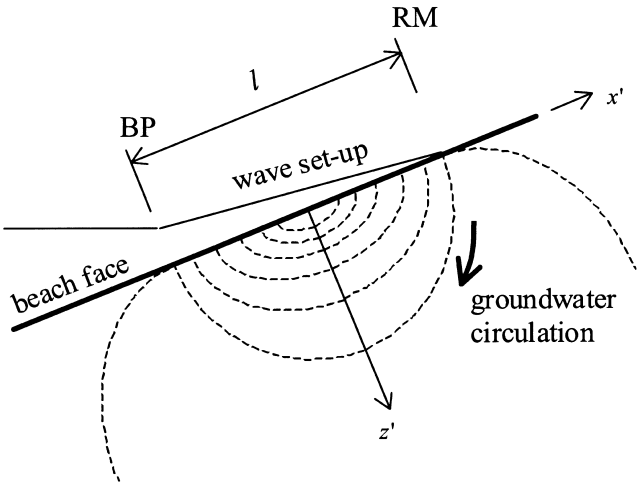

Fig. 17. Schematic diagram of ideal groundwater circulation due to wave set-up [2]. Dashed curves are streamlines.

internal circulation, linked with the water table, did not lead to a net groundwater flow. It is also interesting to note that seaward of the BP, small rates of infiltration existed as a result of wave set-down, although this is difficult to discern in the figure.

The non-dimensional total inflow (i.e., the sum of infiltration rate times the area normalised by K) was calculated to be 0.37 m^2/m along-shore distance and the total outflow (i.e., the sum of exfiltration rate times the area normalised by K) 0.36 m^2/m. Although the former is slightly larger than the latter, the result indicates that the net groundwater flow in the aquifer is relatively small, in accordance with the small difference in hydraulic heads between the landward and seaward boundaries. According to Eqs. (6a)–(6d), the non-dimensional total inflow and outflow rates are the same and both equal sl. To calculate the analytical prediction of the total inflow/outflow rate, we estimated l to be 15 m and used the averaged slope of the mean sea level between BP and RM, i.e., $s = 0.036$. The resulting value

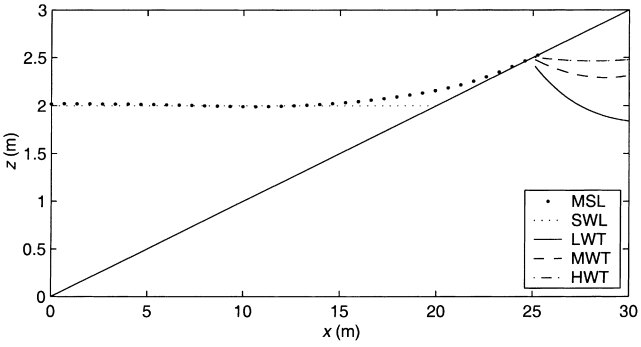

Fig. 18. Comparison of the water tables in the simulations. MSL is the mean sea level, SWL is the initial still seawater level, LWT is the low water table in SIM 3, MWT is the medium water table in SIM 1 and HWT is the high water table in SIM 2.

was 0.54 m^2/m along-shore distance, larger than the numerical data. The effects of the water table, the aquifer's bottom and landward boundaries have reduced the rate of the beach groundwater circulation as induced by wave set-up. Nevertheless, the analytical solution provided an approximate estimate of the infiltration/exfiltration rates.

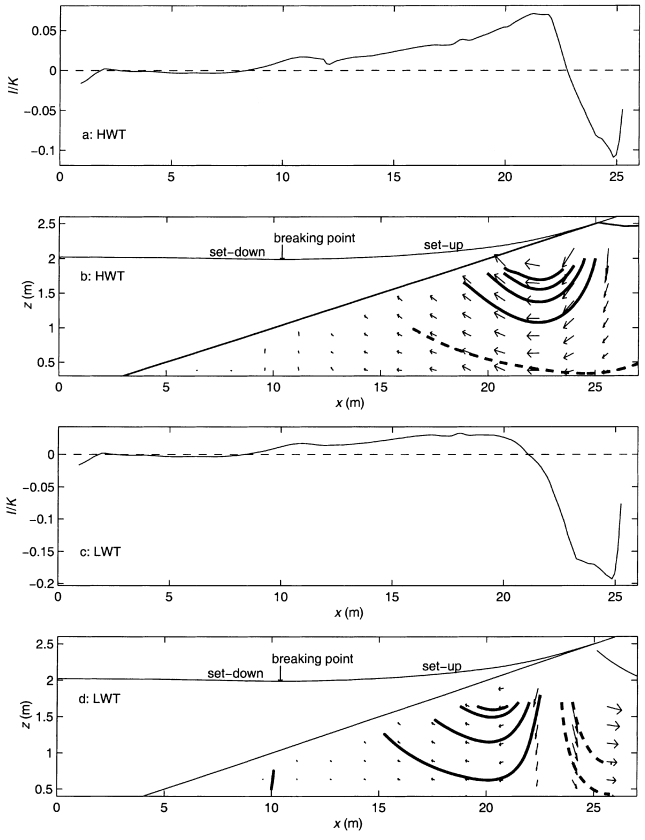

Fig. 19. (a) Averaged infiltration/exfiltration rates from SIM 2 with a HWT. (b) Averaged beach groundwater flow and circulation due to wave set-up from SIM 2. (c) Averaged infiltration/exfiltration rates from SIM 3 with a LWT. (d) Averaged beach groundwater flow and circulation due to wave set-up from SIM 3.

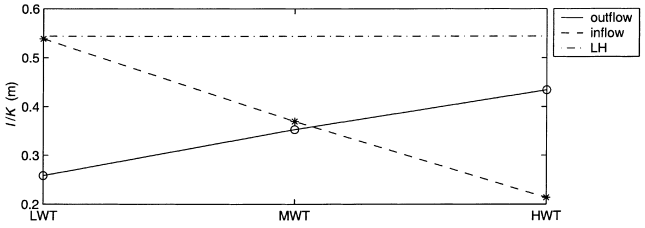

Fig. 20. Variations of the non-dimensional total infiltration/exfiltration rates with the water table elevations. The analytical prediction (LH) is also shown.

To further examine the boundary effects, we conducted another two simulations with high and low hydraulic head conditions at the aquifer's landward boundary, respectively. A comparison of the beach water tables in the three simulations is shown in Fig. 18 together with the mean sea level. The wave conditions were kept the same as in the first simulation. The simulation results of the averaged infiltration/exfiltration rates and the circulation patterns are shown in Fig. 19. It is clear that a high water table reduced the infiltration at the upper part of the beach and increased the exfiltration at the lower part of the beach (Fig. 19a). The circulation cells were moved towards the upper part of the beach (Fig. 19b). A net seaward groundwater flow was evident, which also contributed to the outflow across the beach face (indicated by the dashed path-line in Fig. 19b). Conversely, the low water table enhanced the infiltration and reduced the exfiltration (Fig. 19c). The circulation cells moved seaward. Parts of the infiltration contributed to a net landward groundwater flow (indicated by the dashed path-lines in Fig. 19d). In summary, the effects of the aquifer's free surface and landward boundary conditions affect the phase-averaged beach groundwater flow.

The variations of the non-dimensional total inflow and outflow rates with the water table elevations are shown in Fig. 20. Again, it is clearly evident that the high water table led to an increase in exfiltration and decrease of infiltration; and the opposite occurred due to the low water table. Also plotted in the figure is the analytical estimate of the total inflow/outflow rate. The results show that, in the high and low water table cases, the analytical solution was not adequate for predicting the differences between in- and out-flow rates.

4. Conclusions

We have studied the wave-induced beach groundwater flow in details for a representative beach using numerical modelling. The results revealed important features of this flow:

1. The instantaneous flow is characterised by bore-induced infiltration and exfiltration across the local beach face below the bore. The infiltration–exfiltration flow pattern propagates across the shore with the bore.
2. At the lower part of the beach, the rate of bore-induced flow and its depth variations are related to the square of the bore amplitude and are also affected by the bore front water depth and local aquifer thickness, similar to the behaviour of bore-induced groundwater flow on a flat horizontal bed of a shallow aquifer [6]. At the upper part of the beach, the magnitude of bore-induced flow is related to the bore amplitude linearly.

3. The bore-induced infiltration and exfiltration rates can be relatively large, and may affect sediment transport in the surf zone. In particular, the exfiltration exerts onto the sediment an upward force, which can amount to one third of the sediment's immersed weight.
4. In the swash zone, infiltration is the dominant process and persists with a steady rate while the swash lens overtops the beach face. Exfiltration occurs with a small magnitude and for a short period when the swash depth is zero.
5. Phase-averaged beach groundwater flow is characterised by a groundwater circulation driven primarily by the wave set-up as analysed by Longuet-Higgins [4]. Conditions at the aquifer's free surface, bottom and landward boundaries are also important in determining the circulation.

Although these findings were obtained for a single beach, they have implications for other beaches. Previous studies have shown that the beach groundwater flow may affect considerably sediment transport and chemical exchanges between the aquifer and the ocean. The details of this flow revealed here will assist future studies to quantify its effects on other coastal processes.

Appendix A. Model description

Wave motion on the beach is modelled using the modified depth-averaged non-linear SWE [5], i.e.,

$$\frac{\partial \eta}{\partial t} + \frac{\partial}{\partial x}(\eta u_w) = 0, \tag{A.1a}$$

$$\frac{\partial}{\partial t}(\eta u_w) + \frac{\partial}{\partial x}\left(\eta u_w^2 + \frac{1}{2} g \eta^2\right) = -\tan(\beta) g \eta - \frac{1}{2} f u_w |u_w|, \tag{A.1b}$$

where η is the water depth, u_w the water flow velocity, t the time, x the horizontal coordinate (cross-shore direction), β the beach angle (Fig. 1), g the magnitude of gravitational acceleration, and f is the friction factor.

A dissipative finite difference scheme based on the Lax-Wendroff conservation method is used for solving the SWE [4]. A prescribed incoming wave is combined with the reflective wave (calculated from the numerical solution based on the linear wave theory) to determine the seaward boundary conditions. At the landward side is the shoreline, a moving boundary [5]. A special procedure developed by Hibberd and Peregrine [4] is applied to determine the moving shoreline for every time step.

Beach groundwater is governed by the Laplace equation,

$$\frac{\partial^2 \phi}{\partial x^2} + \frac{\partial^2 \phi}{\partial z^2} = 0, \tag{A.2}$$

where ϕ is the hydraulic head, $= P/\rho g + z$ (P is the pressure, ρ the water density and z is the vertical coordinate). Note that the aquifer has been assumed homogeneous. Such an assumption may not apply strictly at natural beaches. However, it simplifies the complicated modelling to a workable extent in the first instance. Capillary effects are included in a modified free surface boundary condition for the water table,

$$\frac{\partial \phi}{\partial t} = -\frac{K}{n_e \cos(\gamma)} \frac{\partial \phi}{\partial n} - \frac{B_c}{n_e \cos(\gamma)} \frac{\partial}{\partial t}\left(\frac{\partial \phi}{\partial n}\right), \quad z = \eta_g(x,t), \tag{A.3}$$

where K and n_e are the hydraulic conductivity and effective porosity of beach sand, respectively. n is the local coordinate on the boundary (i.e., the water table, $z = \eta_g$) in the normal direction outward from the flow domain, B_c is the thickness of the capillary fringe and γ is the angle between the water table and the horizontal axis. The first and second terms on the right hand side of Eq. (A.3) represent two mechanisms for coastal groundwater responses to the oceanic oscillations [6].

In addition to the water table, three other boundaries exist (Fig. 1): the landward boundary, the seaward boundary (i.e., the beach face) and the impermeable boundary at the base. The landward boundary condition is prescribed by a constant head (i.e., constant potential). At the base, the flux is zero and hence, $\partial\phi/\partial n = 0$. The boundary conditions at the beach face are more complicated. Depending on whether the shoreline and the exit point of the water table couple with each other, a seepage face may exist where $\phi = z$. Seaward of the shoreline, $\phi = \eta + z$ where η is calculated by the SWE. Once the boundary conditions are determined, Eq. (A.2) can be solved using a variety of numerical techniques. The boundary element method is used in this study.

The model is two-dimensional, and thus assumes that the along-shore variations negligible. This assumption is applicable at most beaches where the oblique angle of approaching waves is small due to wave refraction [2].

References

[1] Baird AJ, Horn DP. Monitoring and modelling groundwater behaviour in sandy beaches. J Coastal Res 1996;12:630–40.
[2] Dean RG, Dalrymple RA. Water Wave Mechanics for Engineers and Scientists. World Scientific: Singapore, 1991:353.
[3] Grant US. Influence of the water table on beach aggradation and degradation. J Mar Res 1948;7:655–60.
[4] Hibberd S, Peregrine DH. Surf and runup on a beach a uniform bore. J Fluid Mech 1979;95:323–45.
[5] Kobayashi N, Otta AK, Roy I. Wave reflection and run-up on rough slopes. J Water Port Coastal Ocean Eng ASCE 1987;113:282–98.
[6] Li L, Barry DA, Parlange J-Y, Pattiaratchi CB. Beach water fluctuations due to wave runup: Capillarity effects. Water Resour Res 1997;33:935–45.

[7] Li L, Barry DA, Stagnitti F, Parlange J-Y. Submarine groundwater discharge and associated chemical input to a coastal sea. Water Resour Res, in press.
[8] Longuet-Higgins FRS. Wave set-up, percolation and undertow in the surf zone. Proc R Soc London A 1983;390:283–91.
[9] Martin CS, Aral MM. Seepage force on interfacial bed particles. J Hydraul Div ASCE 1971;7:1081–100.
[10] Masselink G. Morphodynamics of macrotidal beaches: Examples from central Queensland, Australia. Ph.D. Dissertation, Department of Geography, University of Sydney, 1994:272 pp.
[11] Packwood AR. Peregrine DH. The propagation of solitary waves and bores over a porous bed. Coastal Eng 1979;3:221–42.
[12] Parlange J-Y, Brutsaert W. A capillary correction for free surface flow of groundwater. Water Resour Res 1987;23:805–8.
[13] Stoker J. Water Waves. Interscience Publishers: New York, 1957.
[14] Turner IL. Simulating the influence of groundwater Seepage on sediment transport by the sweep of the swash zone across macrotidal beaches. Mar Geol 1995;125:153–74.
[15] Turner I, Masselink G. Swash infiltration–exfiltration and sediment transport. J Geophys Res 1998;103:30813–24.